Original Article

Institution of MECHANICAL ENGINEERS
Journal of MECHANICAL ENGINEERING SCIENCE

Proc IMechE Part C:
J Mechanical Engineering Science
2016, Vol. 230(20) 3777–3790

DOI: 10.1177/0954406215616415
pic.sagepub.com
SAGE

Development and analysis of a gravity-balanced exoskeleton for active rehabilitation training of upper limb

Qingcong Wu, Xingsong Wang and Fengpo Du

Abstract

Robot-assisted therapy has become an important technology applied in rehabilitation engineering, allowing patients with motion impairment problems to perform training programs without continuous supervision from physiotherapists. The goal of this paper is to develop a gravity balanced exoskeleton for active rehabilitation training of upper limb. The mechanical structure and kinematics of the exoskeleton are described and optimized to enable natural interaction with user and avoid singular configurations within the desired workspace. The gravity balancing of the human arm and mechanism is achieved through a hybrid strategy making use of auxiliary links and zero-free-length springs to balance the effect of gravity over the range of motion. The balance errors resulting from the variation of anthropometric parameters are analyzed and discussed. Further experiments involving trajectories tracking tasks with and without gravity balancing are conducted to evaluate the improvement of the control performance and energetic efficiency made by the developed balanced mechanism. The experimental results indicate that the proposed balance strategy can achieve a reduction of 34.56% in overall power consumption compared with the cost in unbalanced condition.

Keywords

Gravity balanced, exoskeleton, active rehabilitation, upper limb, balance errors, power consumption

Date received: 8 August 2014; accepted: 30 July 2015

Introduction

Stroke is a severe neurological disease harming a large number of aged people, leading to significant residual physical and cognitive impairment problems. In terms of the statistical data of the World Health Organization, currently, more than 15 million individuals suffer from the effects of stroke in the world, and there are three million new occurrences every year.[1] Stroke accounts for nearly 10% of all deaths worldwide. Only approximately two-thirds of the stroke population survive and, however, require a prolonged physical therapy to amend functional outcomes and improve movement coordination in activities of daily living (ADL). Studies in clinical treatment have proved that performing sensorimotor movement has positive effects on the motor capability recovery of the impaired limb and, in addition, prevent muscle atrophy and joint spasticity.[2,3] Traditionally, physiotherapists assist the disabled patients to practice different types of multi-joint training programs base on their subjective end-feeling and experience, such as manual guidance training, force-coordination training, and progressive resistive training. This conventional method is widely applied with beneficial results and, however, several obvious drawbacks simultaneously. The therapist treatment is costly and labor-intensive, as it requires one-on-one treatment and, the training durations always take a lot of time. The therapists may get tired or injured easily when manually moving heavy limbs and the therapy effects may not be lasting.[4,5]

Compared with the physiotherapy relying on manual manipulation of the therapist, the robot-assisted therapy is a unique solution capable of delivering high-intensity training and ensuring consistency and efficiency during pertinent rehabilitation treatment. It has garnered significant interest and attention in recent years. Robotic systems can provide effective assistance with various kinds of compensatory movements and, moreover, allowing the therapists to monitor the rehabilitation progress and adjust the training plans reasonably to maximize the quality of treatment. In the last decade, many research groups have developed different kinds of upper-limb robots

Southeast University, Nanjing, Jiangsu Province, China

Corresponding author:
Xingsong Wang, College of Mechanical Engineering, Southeast University, Jiangsu Province, Nanjing 211189, China.
Email: xswang@seu.edu.cn

for the disabled individuals. The effectiveness of the robot-assisted therapy on motor recovery has been analyzed and verified.[6] The existing robotic systems for upper-limb rehabilitation can be basically classified into two categories according to their assistive capabilities as either active or passive devices.

The active, i.e. motorized, rehabilitation devices are equipped with different types of actuators, such as electrical motors, hydraulic cylinders and artificial muscles, and thus able to assist impaired arm movements in programmable training strategies with any level of assistance. For example, the MIT-Manus is a motor-driven robotic rehabilitation manipulator with two degrees of freedom (DOFs) developed by Massachusetts Institute of Technology. It can provide assistance for the elbow, forearm, and wrist movement by guiding the hand of the patient in the horizontal plane and achieves desired force, stiffness and impedance at the end-effector.[7] California Irvine University developed a pneumatically-actuated exoskeleton, named BONES, for the physiotherapy and training of the elbow and shoulder. The original characteristic of this device is the use of the parallel mechanism that actuates the upper-extremity via a fifth cylinder and two sliding rods pivoting with respect to a fixed structural frame. Such a parallel actuation strategy matches the capabilities of the human arm in terms of strength and force-control ability.[8] The ARMin is a semi-exoskeletal rehabilitation device developed to improve the performance of neuromuscular treatment and increase the therapeutic progress in clinics. The device is equipped with DC motors, encoders and force/torque sensors and able to deliver patient-cooperative training strategies.[9] In addition, many other active therapy devices have been designed, such as L-Exos,[10] RehabRoby,[11] IntelliArm,[12] MGA,[13] and GENTLE/s.[14] These actively powered devices are all equipped with driving elements and, as a result, have some disadvantages in common, such as heavy weight, high inertia, large power consumption, and potential fail-safe problems.

The passive, i.e. non-motorised, rehabilitation devices usually make use of elastic bands, springs, weights, auxiliary links and overhead slings to achieve gravity balancing, allowing patients to perform therapy training without robotic actuation.[15–19] The T-WREX is a passive wheelchair exoskeleton developed by Sanchez et al.[20] This five DOFs upper-limb mechanism is identically gravity balanced for the weight of user with rubber bands wrapped around two four-bar linkages. The Dampace is a resistive device making use of disk brakes to apply controlled resistance torque on the shoulder and elbow joints. The weight of the robotic system is compensated by a balanced spring mechanism.[21] The ARMON is a non-powered orthosis developed in Delft University of Technology. This device is statically balanced by a balancer consisting of non-circular cams, pulleys, cables, and springs.[22] Using passive devices has the advantages of lightweight implementation, low power consumption, and inherent safety. However, it can only apply a few fixed patterns of therapy, leading to limited recovery performance. Besides, it is difficult for the seriously disabled patients to actively complete the therapy training due to the unavoidable balancing errors and friction.

Taking the above into account, a motorized version of gravity balanced robot is a preferred option that can effectively combine the advantages of the active assistant devices and the passive ones. Therefore, the purpose of the current study is to develop a gravity balanced exoskeleton with active actuators, named AGB-Exo, for the rehabilitation of shoulder and elbow. The device is equipped with DC servo motors and flexible Bowden-cable transmission systems in order to provide active assistance and achieve improved motion control. Auxiliary parallel links and zero-free-length springs, i.e. the rest lengths of the springs are zero,[23] are incorporated into the exoskeleton to balance the gravity forces acting on the human arm and device. This paper first provides a description of the mechanical design and the kinematics of the exoskeleton. And then the principle of gravity balance and the balance errors resulting from the variation of anthropometric parameters are analyzed. Finally, this paper reports the comparisons of the trajectories tracking experiments with and without gravity balancing.

Design of the exoskeleton

Mechanical design

For good performance of therapy training, the mechanical structure of the rehabilitation device is designed to be kinematically similar to the human arm anatomy. The architecture of the exoskeleton is shown in Figure 1. It comprises three active DOFs to enable spatial shoulder movements, i.e. internal/external, abduction/adduction and flexion/extension, one active DOF to enable elbow flexion/extension movement, and one passive DOF at the elbow permitting pronation/supination movement of the forearm. However, it should be noted the human shoulder complex has two DOFs at the sternoclavicular joint and three DOFs at the glenohumeral joint. It is unreasonable to simply approximate the shoulder as a spherical joint, as the rotation center of glenohumeral joint shifts according to shoulder girdle movement, and the undesired misalignment between human and robot will cause uncontrollable forces imposed on the user.[24,25] For this reason, in order to provide proper glenohumeral motion, the exoskeleton is placed on a mobile platform mechanism with two passive DOFs to compensate the misalignment in the horizontal directions.

For each active joint of the exoskeleton, the driving torque is delivered from a servo brushless DC motor

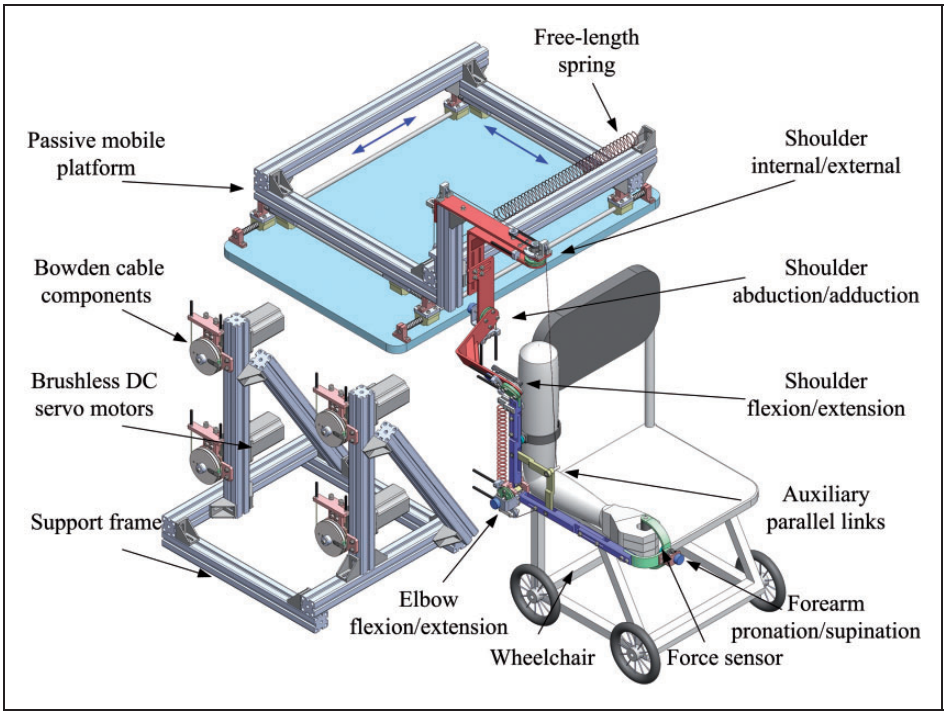

Figure 1. The architecture and major components of the rehabilitation exoskeleton.

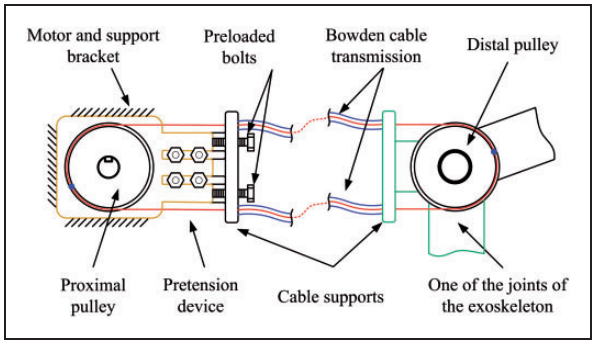

Figure 2. Schematic of the Bowden-cable actuation system.

via a flexible Bowden-cable transmission system, as shown in Figure 2. The cables are attached to the proximal pulley and distal pulley in a pull-pull configuration, ensuring that the robotic joint can rotate consistently with the motion of actuator in both directions. The pretension device can be used to adjust the system pretension and eliminate slacking due to cable elasticity. The servo motors, able to exert a maximum continuous torque of 35 Nm, are located at a fixed frame remote from the exoskeleton. Such an arrangement helps to reduce the weight and volume of the moving parts.

The position of each robot joint is measured with a conductive plastic angle potentiometer enclosed in the joint structure. To incorporate the human-robot interactive force into rehabilitation training, a six-dimensional force/torque sensor is attached to the end-effector to detect the forces between the hand of the user and the palm handle. The lengths of the exoskeleton segments are designed to be tunable so that the device can be adapted to patients of different anthropometric parameters. A custom-made cuff is attached to the upper arm of AGB-Exo to ensure a comfortable connection between the user and the exoskeleton. A wheelchair is placed in front of the platform, allowing the user to be seated comfortably while executing the training task. For safety consideration, mechanical end stoppers are mounted on each joint to protect the patient from excessive rotation and extension. Besides, both of the patient and the therapist are required to hold an emergency stop button in their hands so that the robotic system can be shut down immediately in dangerous situation. As the device is developed with gravity compensation, the system does not collapse after power loss.

Configuration space kinematics

The kinematics of AGB-Exo is presented in Figure 3. The Denavit-Hartenburg (D-H) method[26] is applied to describe the robot coordinate frames. The robot D-H parameters are summarized in Table 1. We can see that the rehabilitation exoskeleton achieves nearly all the ranges of movement required to perform daily activities. It should be noted that the base coordinate frame is moved from the experimental platform to the internal/external joint of the shoulder, as the movement range of the passive mobile platform is fairly small during rehabilitation training, and choosing the platform as the base coordinate frame, however, will greatly increase kinematics complexity. Then the configuration of the exoskeleton can be determined according to the D-H parameters and space

kinematics. The transformation matrix from the base coordinate frame to the end-effector can be given by

$$ {}^{b}T_{e} = {}^{b}T_{2}(\theta_1)^{2}T_{3}(\theta_2)^{3}T_{4}(\theta_3)^{4}T_{5}(\theta_4)^{5}T_{e}(\theta_5) \quad (1) $$

where ${}^{i}T_{j}$ represents the transformation matrix for transition from the i coordinate frame to the j. θ_j denotes the joint rotation variable. The forward kinematics is a function of joint variables and limb lengths L_1 and L_2.

Singularity placement

For the upper-limb exoskeleton, a potential problem with the shoulder movement is that singular configurations occur when two of the shoulder axes become collinear and, as a result, a DOF will be lost. Therefore, the singularities should be eliminated from the desired accessible workspace. For the purpose of optimizing the mechanical design and maximizing the available workspace, a simple method has been developed to calculate the singularity level W of each configuration.[5] The singularity level can be defined as

$$ \mathrm{W} = 1 - \left|\mathbf{z_1} \cdot (\mathbf{z_2} \times \mathbf{z_3})\right| \quad (2) $$

where $\mathbf{z_i}$ denotes the unit vector of each joint axe. When $\mathrm{W} = 0$, the joint axes are orthogonal and the manipulability of the mechanism is maximized; on the contrary, a DOF is lost when $\mathrm{W} = 1$, as a result of the alignment of two joint axes.

An initial prototype has been developed in our previous research with the three shoulder axes mutually perpendicular to each other. However, such a structure has a limited workspace smaller than the ranges of movement of the shoulder in ADL, as the singularity can be reach through abduction by 90°. In order to place the singularities in the boundaries of the desired workplace, the optimized design represented in this paper is developed with the third shoulder axis mounted at an angle of 30° from the horizontal plane, as shown in Figure 3. Figure 4 shows the comparison of the singularity level distribution of the elbow in the previous design and the optimized design. Point S represents the spherical joint of the shoulder. It is clear to see that the location points with high singularity level have been removed from the center to the top of the workplace in the optimized design. Thus the optimized strategy is better than the previous one.

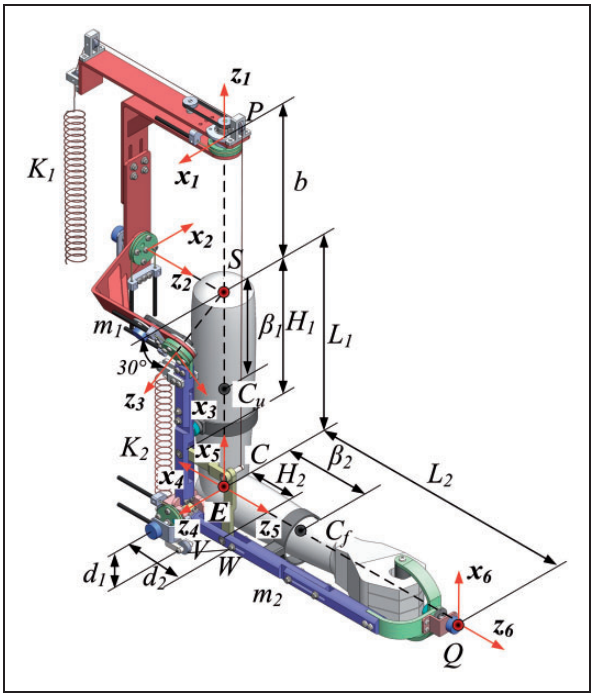

Figure 3. Kinematics and parameters of the exoskeleton with human arm.

Principle of gravity balance

A device is said to be gravity balanced if the considered system keeps in static equilibrium at any reachable configurations.[19] One kind of mathematical descriptions for gravity balanced can be represented as: the total potential energy remains invariant over the range of its motion. The gravity balance principle of AGB-Exo is developed based on the hybrid method proposed by Agrawal and Fattah.[15] Firstly, auxiliary links are utilized to geometrically locate the center of mass (COM) of the human arm and exoskeleton. And then, the zero-free-length springs, made up of tension springs, cables and pulleys, are mounted at suitable positions in order to balance the effect of gravity and

Table 1. Denavit-Hartenburg parameters for the upper-limb exoskeleton.

Link i	θ_i/home (deg)	α_i (deg)	a_i (mm)	d_i (mm)	ROM_ADL (deg)	ROM_EXO (deg)
1	Θ_1/180	90	0	0	130 ~ 245	150 ~ 240
2	Θ_2/−60	90	0	0	−195 ~ −35	−180 ~ −45
3	θ_3/−90	30	0	$L_1/2$	−135 ~ 45	−120 ~ 30
4	θ_4/−90	90	0	0	−180 ~ −45	−180 ~ −30
5	θ_5/0	0	0	L_2	−90 ~ 75	−85 ~ 60

ROM: ranges of movement; ADL: activities of daily living.

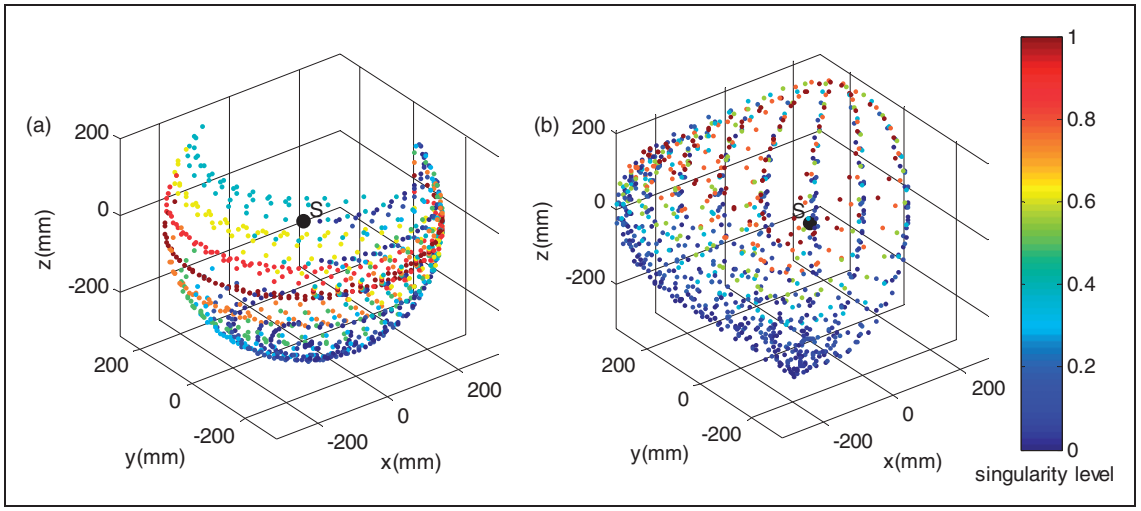

Figure 4. The available workspace and singularity level distribution of the elbow: (a) previous design; (b) optimized design.

keep potential energy invariant with all configurations. Figure 3 shows the integrated view of the exoskeleton combining with human arm. The shoulder joints of the robot and user are coincident at point S. It is worth noting that the forearm pronation/supination DOF can be neglected when developing the balance model, as the forearm is generally axial symmetry and, therefore, the pronation/supination movement has little effect on the variation of potential energy. Parameters shown in Figure 3 are described as follow:

m_1, m_2 masses of the upper arm and forearm (include the robot arm and human arm);
L_1, L_2 lengths of the upper arm and forearm;
C_u, C_f, C the COM of the upper arm, forearm and the whole arm;
β_1, β_2 distances from the COM of upper arm and forearm to the previous joint;
K_1, K_2 two zero-free-length springs;
k_1, k_2 stiffness of the corresponding spring;
d_1, d_2 distances from the connection pointes of springs to the elbow joint;
H_1, H_2 distances from the connection pointes of auxiliary links to the previous joints;
$\mathbf{x_i}$, $\mathbf{y_i}$, $\mathbf{z_i}$ unit vector of the ith coordinate axes;
S, E, Q shoulder joint, elbow joint and end-effector;
b distance between point P and S.

The gravitational potential energy of the upper limb can be expressed as

$$V_g = -\left(m_1\mathbf{g}\cdot\mathbf{r}_{SC_u} + m_2\mathbf{g}\cdot\mathbf{r}_{SC_f}\right) = -(m_1+m_2)\mathbf{g}\cdot\mathbf{r}_{SC} \tag{3}$$

where $\mathbf{r}_{SC_u}$, $\mathbf{r}_{SC_f}$ and $\mathbf{r}_{SC}$ denote the position vectors from the shoulder joint to the COM of the upper arm, forearm and the entirety arm. $\mathbf{g}$ represents the gravitation vector. According to the Cartesian coordinate systems shown in Figure 3, these vectors can be written as

$$\mathbf{g} = -g\mathbf{z}_1 \tag{4}$$

$$\mathbf{r}_{SC_u} = \beta_1\mathbf{y}_4 \tag{5}$$

$$\mathbf{r}_{SC_f} = L_1\mathbf{y}_4 + \beta_2\mathbf{z}_5 \tag{6}$$

$$\mathbf{r}_{SC} = \frac{m_1\mathbf{r}_{SC_u} + m_2\mathbf{r}_{SC_f}}{m_1+m_2} = \frac{m_1\beta_1 + m_2L_1}{m_1+m_2}\mathbf{y}_4 + \frac{m_2\beta_2}{m_1+m_2}\mathbf{z}_5 \tag{7}$$

For simplification, we define

$$H_1 = \frac{m_1\beta_1 + m_2L_1}{m_1+m_2}, \quad \text{and} \quad H_2 = \frac{m_2\beta_2}{m_1+m_2}$$

Thus, equation (7) can be refined as

$$\mathbf{r}_{SC} = H_1\mathbf{y}_4 + H_2\mathbf{z}_5 \tag{8}$$

In order to locate the system COM, the exoskeleton is equipped with two auxiliary links parallel to the upper arm and forearm, respectively. The length of the auxiliary link parallel to the upper arm is L_1-H_1, while the other one is H_2. According to equation (8) and Figure 3, it is clear to see that the location of the system COM can be determined by the coincident joint of auxiliary links, i.e. point C, in any configuration.

Inserting equation (7) into equation (3), the gravitational potential energy can be refined as

$$V_g = (m_1g\beta_1 + m_2gL_1)\mathbf{z}_1\cdot\mathbf{y}_4 + m_2g\beta_2\mathbf{z}_1\cdot\mathbf{z}_5 \tag{9}$$

Note that the value of V_g is changed with the upper-limb configuration. For gravity compensation, two zero-free-length springs K_1 and K_2 are attached to

the points P, C and V, W, respectively. The strain potential energy of the zero-free-length springs can be shown as

$$V_s = \sum_{i=1}^{2} k_i D_i^2 \tag{10}$$

Here D_i denotes the extended length of ith spring and can be computed by

$$D_1^2 = \|\mathbf{PC}\|^2 = \left(-b\mathbf{z}_1 + H_1\mathbf{y}_4 + H_2\mathbf{z}_5\right)^2 \tag{11}$$

$$D_2^2 = \|\mathbf{VW}\|^2 = \left(d_2\mathbf{z}_5 - d_1\mathbf{y}_4\right)^2 \tag{12}$$

Upon substitution of equations (11) and (12) into equation (10), the strain potential energy can be refined as

$$\begin{aligned} V_s = {} & \frac{1}{2}k_1(b^2 + H_1^2 + H_2^2) + \frac{1}{2}k_2(d_1^2 + d_2^2) \\ & - k_1 b H_1 \mathbf{z}_1 \cdot \mathbf{y}_4 - k_1 b H_2 \mathbf{z}_1 \cdot \mathbf{z}_5 \\ & + (k_1 H_1 H_2 - k_2 d_1 d_2)\mathbf{y}_4 \cdot \mathbf{z}_5 \end{aligned} \tag{13}$$

The total potential energy is the sum of potential energies of gravity and springs, thus we get

$$\begin{aligned} V = {} & V_g + V_s \\ = {} & \frac{1}{2}k_1(b^2 + H_1^2 + H_2^2) \\ & + (m_1 g\beta_1 + m_2 L_1 g - k_1 b H_1)\mathbf{z}_1 \cdot \mathbf{y}_4 \\ & + \frac{1}{2}k_2(d_1^2 + d_2^2) + (m_2 g\beta_2 - k_1 b H_2)\mathbf{z}_1 \cdot \mathbf{z}_5 \\ & + (k_1 H_1 H_2 - k_2 d_1 d_2)\mathbf{y}_4 \cdot \mathbf{z}_5 \end{aligned} \tag{14}$$

The values of k_1, k_2 are selected to keep the total potential energy unchanged with all configurations. Setting the stiffness of the springs as follows

$$k_1 = \frac{(m_1 + m_2)\, g}{b} \tag{15}$$

$$k_2 = \frac{k_1(m_1\beta_1 + m_2 L_1)m_2\beta_2}{(m_1 + m_2)^2 d_1 d_2} = \frac{k_1 H_1 H_2}{d_1 d_2} \tag{16}$$

Substitution of equations (15) and (16) into equation (14) yields

$$V = \frac{1}{2}k_1(b^2 + H_1^2 + H_2^2) + \frac{1}{2}k_2(d_1^2 + d_2^2) = \text{constant} \tag{17}$$

Note that the total potential energy becomes configuration-invariant with the spring stiffnesses given by equations (15) and (16). Therefore, the gravity balancing is achieved.

The residual torque, defined as the summation of the gravitational torque and the compensational torque generated by the springs, acting on the ith joint can be computed by differentiating the total potential energy equation with respect to the joint rotation variable θ_i

$$\tau_i = \frac{\partial V}{\partial \theta_i} \quad i = 1, 2, 3, 4 \tag{18}$$

Equation (18) indicates that the driving torque required to overcome the gravity effect become zero when the exoskeleton operates in gravity balanced condition.

Balance errors of the exoskeleton

The exoskeleton and human arm are regarded as a combinative system during the development process of the balance model. The rehabilitation device should be applicable to different individuals in practical application. As seen from equations (8), (15), and (16), in order to achieve completely gravity balancing, the spring stiffnesses, i.e. k_1 and k_2, and the lengths of the auxiliary links, i.e. L_1-H_1 and H_2, need to be modulated according to the anthropometric parameters of user. However, the adjusting operations are quite complex to complete and, as a result, may introduce balance errors. Therefore, it is necessary to analyze the effects of balance errors resulting from the variation of anthropometric parameters.

According to the anthropometry in movement biomechanics,[27] the segment lengths and segment masses of upper limb and the locations of COM can be expressed as the percentages of body height T and body weight M. The parameters of the exoskeleton can be obtained from the virtual prototype. We consider a user weighting 60 kg and 1.7 m tall. Then, the parameters of the human arm, exoskeleton and the whole entirety are calculated and shown in Table 2.

Table 2. Anthropometric parameters of the human arm and exoskeleton.

Parameters	m_1 (kg)	m_2 (kg)	L_1 (mm)	L_2 (mm)	β_1 (mm)	β_2 (mm)
Anthropometry	0.028M	0.016M	0.186T	0.146T	0.436L_1	0.683L_2
Human arm	1.68	1.32	316	248	137.8	169.3
Exoskeleton	1.45	0.73	316	248	163	216.4
Entirety	3.13	2.05	316	248	149.4	186.1

Applying these parameters into equations (15) and (16), we can get the stiffnesses of springs and the lengths of the auxiliary links: $k_1 = 0.21\,\text{N/mm}$, $k_2 = 0.52\,\text{N/mm}$, L_1-$H_1 = 100.6\,\text{mm}$, $H_2 = 74.6\,\text{mm}$.

If the springs and auxiliary links are not adjustable, balance errors may occur due to the variations of anthropometric parameters. Derived from the D-H transformation matrixes, we can get

$$\mathbf{z}_1 \cdot \mathbf{y}_4 = -\frac{c_2 + \sqrt{3}s_2 s_3}{2} \tag{19}$$

$$\mathbf{z}_1 \cdot \mathbf{z}_5 = \frac{c_2 c_4 + \sqrt{3}s_2 s_3 c_4}{2} + s_2 c_3 s_4 \tag{20}$$

$$\mathbf{y}_4 \cdot \mathbf{z}_5 = -c_4 \tag{21}$$

where $s_i = \sin(\theta_i)$, $c_i = \cos(\theta_i)$. Substituting equations (19) to (21) into equation (14), the total potential energy can be given

$$\begin{aligned} V = {} & \frac{1}{2}k_1(b^2 + H_1^2 + H_2^2) + \frac{1}{2}k_2(d_1^2 + d_2^2) \\ & - (k_1 H_1 H_2 - k_2 d_1 d_2)c_4 + (\mathrm{m'}_2 \mathrm{g}\beta'_2 - k_1 b H_2) \\ & \times \left(\frac{c_2 c_4 + \sqrt{3}s_2 s_3 c_4}{2} + s_2 c_3 s_4\right) - (\mathrm{m'}_1 \mathrm{g}\beta'_1 + \mathrm{m'}_2 L'_1 g \\ & - k_1 b H_1) \times \left(\frac{c_2 + \sqrt{3}s_2 s_3}{2}\right) \end{aligned} \tag{22}$$

where $\mathrm{m'}_1$, $\mathrm{m'}_2$, β'_1, β'_2 and L'_1 represents the actual upper-limb parameters. Note that the springs and auxiliary links are selected for the complete gravity balance of the individual with a weight of 60 kg and a height of 1.7 m tall. Therefore, for the users with different anthropometric parameters, the terms containing trigonometric variables cannot be eliminated from equation (22). Inserting equation (22) into (18) gives the residual torque of each joint resulting from balance error

$$\tau_1 = \frac{\partial V}{\theta_1} = 0 \tag{23}$$

$$\begin{aligned} \tau_2 = {} & \frac{\partial V}{\theta_2} \\ & = (\mathrm{m'}_2 \mathrm{g}\beta'_2 - k_1 b H_2) \times \left(\frac{-s_2 c_4 + \sqrt{3}c_2 s_3 c_4}{2} + c_2 c_3 s_4\right) \\ & - (\mathrm{m'}_1 \mathrm{g}\beta'_1 + \mathrm{m'}_2 L'_1 g - k_1 b H_1) \times \left(\frac{-s_2 + \sqrt{3}c_2 s_3}{2}\right) \end{aligned} \tag{24}$$

$$\begin{aligned} \tau_3 = \frac{\partial V}{\theta_3} = {} & (\mathrm{m'}_2 \mathrm{g}\beta'_2 - k_1 b H_2) \times \left(\frac{\sqrt{3}s_2 c_3 c_4}{2} - s_2 s_3 s_4\right) \\ & - (\mathrm{m'}_1 \mathrm{g}\beta'_1 + \mathrm{m'}_2 L'_1 g - k_1 b H_1) \times \left(\frac{\sqrt{3}s_2 c_3}{2}\right) \end{aligned} \tag{25}$$

$$\begin{aligned} \tau_4 = {} & \frac{\partial V}{\theta_4} \\ & = (\mathrm{m'}_2 \mathrm{g}\beta'_2 - k_1 b H_2) \times \left(s_2 c_3 c_4 - \frac{c_2 s_4 + \sqrt{3}s_2 s_3 s_4}{2}\right) \\ & + (k_1 H_1 H_2 - k_2 d_1 d_2) s_4 \end{aligned} \tag{26}$$

We can see that the residual torque of the first shoulder joint is identically equal to zero, as the potential energy remains invariant during the shoulder internal/external movement of AGB-Exo.

For the purpose of analyzing and evaluating the error effects, the exoskeleton was required to perform a trajectory tracking task with a circular path parallel to the coronal plane. The initial configuration is defined with the upper arm vertical to the transverse plane and the forearm vertical to the coronal plane, as shown in Figure 3. The position vector from the shoulder to the location of the end-effector can be expressed in the inertial coordinate frame as

$$\mathbf{SQ} = Q_x \mathbf{x_1} + Q_y \mathbf{y_1} + Q_z \mathbf{z_1} \tag{27}$$

Thus, the circle trajectory can be written as

$$Q_x = R\sin(\omega t) \tag{28}$$

$$Q_y = L_2 \tag{29}$$

$$Q_z = R - L_1 - R\cos(\omega t) \tag{30}$$

where R denotes the radius of the circle. ω represents the tracking angular velocity.

To determine the joint parameters for given end-effector configurations, the inverse kinematic model of the exoskeleton was established based on the method developed by Byoung Gook Loh and Jacob Rosen.[28] The joint angles can be obtained as follows

$$\theta_4 = -\left|\mathrm{a}\cos\left(\frac{L_1^2 + L_2^2 - Q_x^2 - Q_y^2 - Q_z^2}{2L_1 L_2}\right)\right| \tag{31}$$

$$\theta_2 = -\mathrm{a}\cos\left(\frac{\left\{\begin{array}{c} L_2 s_4 \sqrt{L_1^2 - 2L_1 L_2 c_4 + L_2^2 - Q_z^2} \\ -L_1 Q_z + L_2 Q_z c_4 \end{array}\right\}}{2L_1^2 - 4L_1 L_2 c_4 + 2L_2^2}\right) \tag{32}$$

$$\theta_3 = \mathrm{actan2}\left(\frac{\sqrt{3}L_2 c_2 s_4}{Q_z - 2L_2 c_2 c_4 + 2L_1 c_2}\right) \tag{33}$$

$$\theta_1 = \mathrm{actan2}\left(\frac{Q_y}{Q_x}\right) - \mathrm{actan2}\left(\frac{\eta}{\sqrt{Q_x^2 + Q_y^2 - \eta^2}}\right) \tag{34}$$

where

$$\eta = \frac{\sqrt{3}L_2c_3c_4}{2} - \frac{\sqrt{3}L_1c_3}{2} - L_2s_3s_4 \tag{35}$$

According to equations (23) to (35), the residual torques caused by the variations of body weight and height can be calculated. Computations were conducted with R and ω set to 0.25 m and $\pi/2$ rad/s, respectively.

Figure 5(a) to (d) shows the time history of residual torques about each active joint during a cycle of tracking motion, with the weight of user changing within the ranges of 50 kg ~ 90 kg. It can be observed that the residual torques in balanced condition turn out to be much smaller than those without gravity balancing, i.e. with the stiffnesses of springs set to zero, when performing the moving task. More specifically, the mean absolute torques fall from 1.82 Nm, 3.50 Nm and 5.11 Nm (unbalanced) to 0.18 Nm, 0.39 Nm and 0.50 Nm (balanced) for shoulder abduction/adduction, flexion/extension, and elbow flexion/extension, respectively.

Figure 6(a) to (d) plots the time history of balance torques about each active joint with the height of user changing from 1.6 m to 2 m. In this case, we can see that the mean absolute torques fall from 1.47 Nm, 3.21 Nm and 4.46 Nm (unbalanced) to 0.12 Nm, 0.15 Nm and 0.13 Nm (balanced) for shoulder abduction/adduction, flexion/extension, and elbow flexion/extension, respectively. The simulation results indicates that the residual torques resulting from weight deviation are much higher than those caused by the height deviation in balanced condition, but both of them are lower than 10% of the unbalanced residual torques. Therefore, the results prove that the balance levels of the rehabilitation device have strong robustness to the variation of anthropometric parameters.

Experimental validation

Experimental setup

The experimental setup of the rehabilitation system was composed of the AGB-Exo robot and a real-time control system established in xPC target environment based on Matlab/RTW, as depicted in Figure 7. The control hardware mainly consisted of two industrial personal computers (IPC-610H/3.0 GHz, Advantech Inc.) working as the host computer and the real-time target, a force/torque sensor (NANO-25, ATI Industrial Automation, manufacturer verified accuracy: 1.5% of full scale load) mounted at the end-effector to acquire the

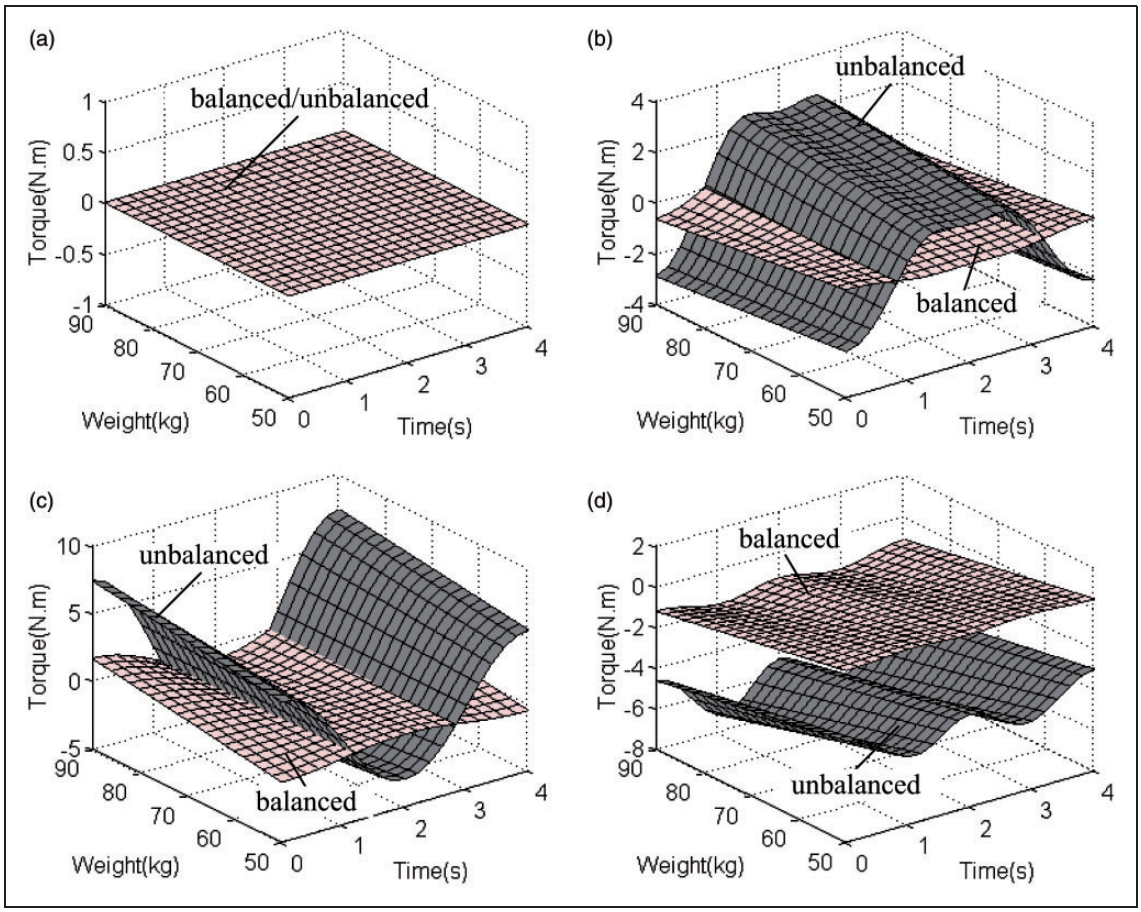

Figure 5. Residual torques of each active joint during tracking motion, with the weight of user changing from 50 kg to 90 kg.

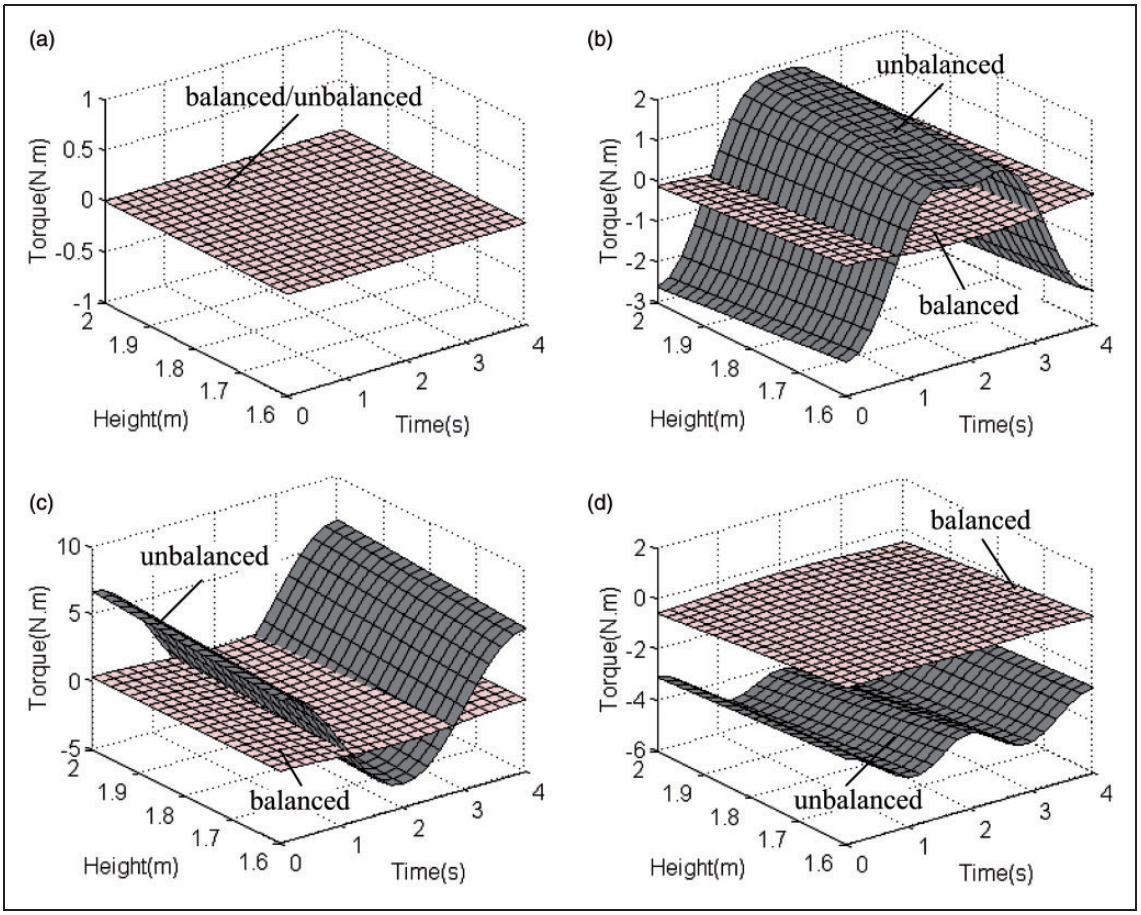

Figure 6. Residual torques of each active joint during tracking motion, with the height of user changing from 1.6 m to 2 m.

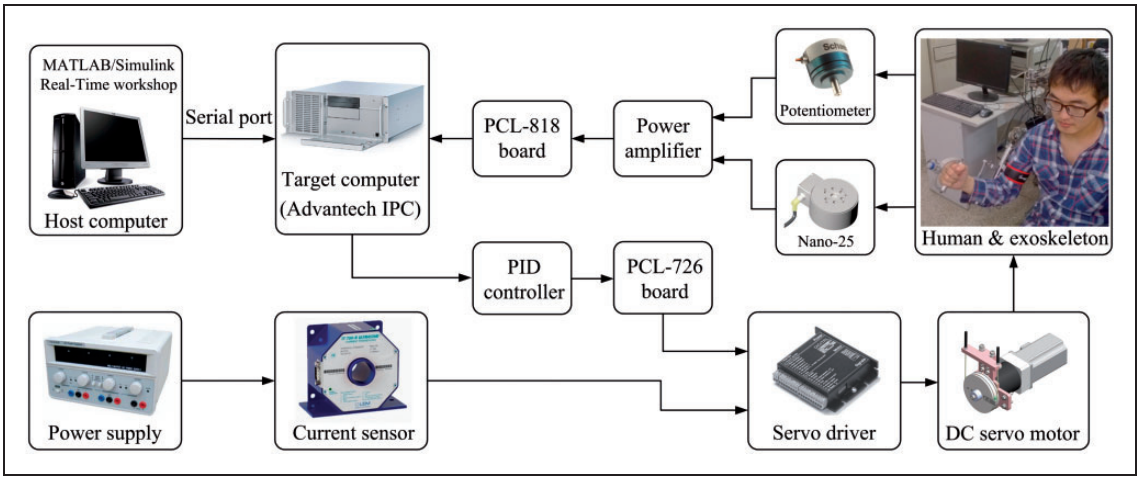

Figure 7. The hardware architecture of the real-time control system.

human-robot interaction forces, four rotary potentiometers (WDJ22A-10K, OMTER Inc., independent linearity: ±1%, electrical rotation: 320° ± 5°) installed at the robot joints to measure the angular positions, and servo drivers (BLDC-5015A, WANTAI Inc.) used in actuation of the brushless DC motors (BLDC-56PA77G-SHJK, reduction ratio-50:1). The servo motors were all run in velocity control mode. The required power was supplied to the motors by two 24 V DC regulated power supplies (WYK-305, Cosyen Inc.). The working current of each motor was detected by a current sensor (HAS50-s, LEM Inc.) with a current measurement resolution of 50 mA and a max measurement error of 100 mA. The signals of the sensors, amplified by a transistor made power amplifier, were acquired and processed via a data acquisition card (PCL-818HD, Advantech Inc.) with an analog input resolution of 12 bits and a max

Table 3. The gain coefficients of the proportional–integral–derivative controllers for different subjects and conditions.

		Balanced				Unbalanced			
Subject	Parameters	Joint 1	Joint 2	Joint 3	Joint 4	Joint 1	Joint 2	Joint 3	Joint 4
Subject 1 (weight: 61 kg, height: 1.7 m)	K_p	1.8	2.7	4.5	2.1	2.3	3.7	5.6	2.6
	K_i	0.6	1.2	2.5	0.3	0.9	0.9	3.0	0.4
	K_d	0.05	0.2	0.23	0.1	0	0.08	0.35	0.1
Subject 2 (weight: 82 kg, height: 1.83 m)	K_p	2.4	3.0	5.0	2.5	3.1	4.1	6.2	3.0
	K_i	0.8	1.6	2.6	0.35	0.8	1.3	3.5	0.5
	K_d	0.05	0.1	0.23	0.1	0.07	0.12	0.35	0.15

Note: Joint 1: shoulder internal/external rotation; Joint 2: shoulder abduction/adduction; Joint 3: shoulder flexion/extension; Joint 4: elbow flexion/extension.

sampling rate of 100 kHz. The control schemes for upper-limb rehabilitation were firstly developed in the host computer in Simulink environment and then transmitted to the real-time target computer through serial port. The acquired analog signals were filtered by using a third-order low-pass Butterworth filter with a cut-off frequency of 40 rad/s. The real-time target was capable of analyzing all the feedback information and sending the appropriate commands to the motor controllers in discrete time. The generated commands were transformed into analog output signals by using a D/A card (PCL-726, Advantech Inc.) with an analog output resolution of 12 bits and a relative accuracy of ±0.012% of full scale range. The control frequency of the real-time system was set to 1 kHz, and the feedback signals from force/torque sensor, rotary potentiometers, as well as current sensors were sampled at the same rate.

Experimental results and analyses

Using a gravity balanced mechanism helps to improve the control performance and the energetic efficiency of the active rehabilitation device, as the energy required to overcome the gravity forces acting on the exoskeleton is reduced or even eliminated. The following experimental protocols were developed to validate the improvement made by the proposed balanced mechanism.

Two healthy neurologically intact subjects with different anthropometric parameters (subject 1: male, weight/61 kg, height/1.7 m; subject 2: male, weight/82 kg, height/1.83 m) participated in this research. Several trajectory tracking experiments were carried out with the subjects passively equipped with the upper-limb exoskeleton. The subjects were instructed to remain totally relaxed and allow the exoskeleton to guide the trajectories of their arms during operation. This means that the driving motor of each robotic joint applied all the necessary torques to perform the tasks. The circular trajectory was predefined with R and ω set to 0.25 m and $\pi/2$ rad/s, respectively. Each of the robotic joints was independently controlled via a proportional–integral–derivative algorithm running in the real-time control system. The gain coefficients of the proportional–integral–derivative controllers were carefully turned by trial and error in order to improve the control performances under different experimental conditions. The relatively favorable gain coefficients of each controller are shown in Table 3. Then the tracking performances of the exoskeleton with and without gravity balancing were compared and analyzed. It should be noted that the unbalanced condition can be achieved by removed the auxiliary springs from the exoskeleton. The experimental data from the potentiometers were made use to calculated the actual location of the end-effector in the inertial coordinate frame based on the forward kinematics. The tracking error is defined as the difference between the actual and the desired position for each point-sampled during tracking motion. The real-time power consumption of each DC motor can be computed as the product of the supply voltage and the working current measured by the current sensor.

Figures 8 and 9 present the experimental results of the circular trajectory tracking tests conducted in balanced and unbalanced condition with different subjects. Figures 8(a) and 9(a) compare the desired and actual motion trajectories projecting onto the plane $Q_y = L_2$. As can be observed, the tracking performance enhanced by gravity balancing has turned out to be far more desirable. The tracking errors are presented comparatively in Figures 8(b) and 9(b), where we can see that the average tracking errors decline from 8.87 mm and 10.92 mm (unbalanced) to 4.17 mm and 5.68 mm (balanced) with subject 1 and subject 2, respectively. Meanwhile, the increases of body weight and height may also lead to larger tracking errors.

Figures 10 and 11 present the time history of power consumption about each actuated joint during a cycle of tracking motion, with and without gravity balancing. It can be seen that, during the experiments conducted with subject 1, the average consumed-powers of shoulder internal/external, abduction/adduction, flexion/extension, and elbow flexion/extension

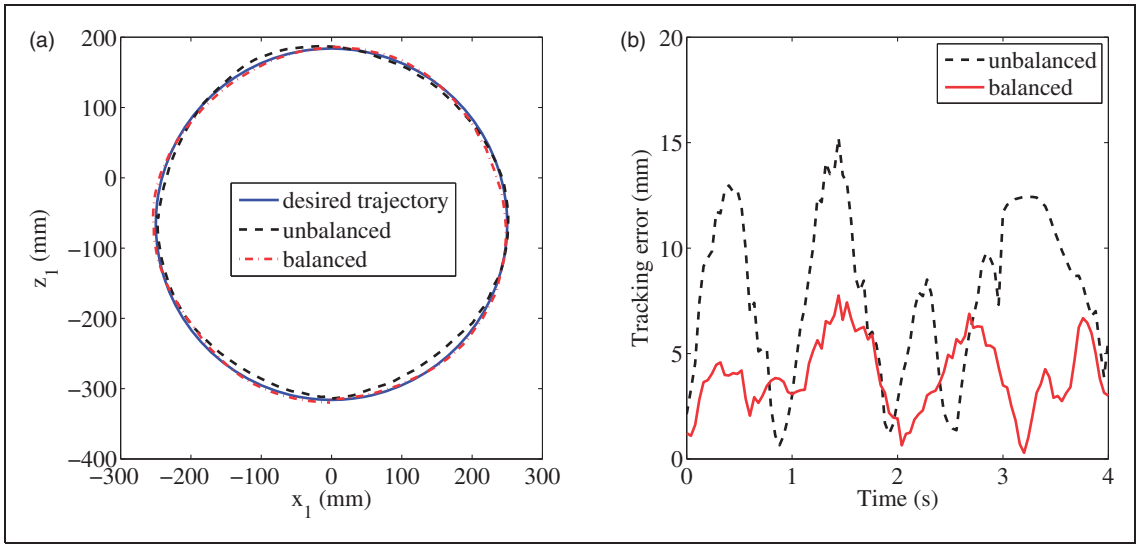

Figure 8. Experimental results of the circular trajectory tracking tests conducted with subject 1: (a) the desired and actual motion trajectories; (b) the tracking errors.

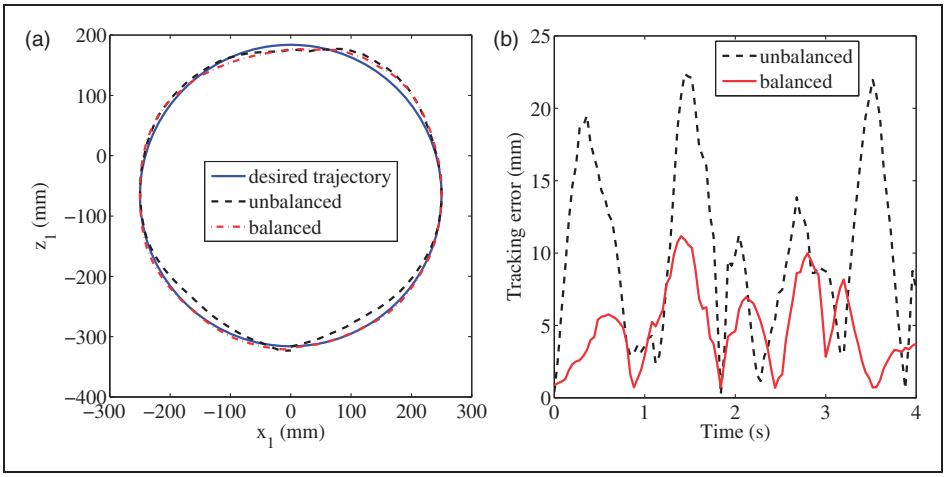

Figure 9. Experimental results of the circular trajectory tracking tests conducted with subject 2: (a) the desired and actual motion trajectories; (b) the tracking errors.

change from 5.73 W, 12.32 W, 19.26 W, and 16.12 W (unbalanced) to 6.12 W, 6.85 W, 10.19 W, and 8.05 W (balanced), respectively. On the other hand, the average consumed-powers of the experiments conducted with subject 2 change from 7.89 W, 16.04 W, 26.16 W, and 21.50 W (unbalanced) to 7.46 W, 11.53 W, 18.98 W, and 12.58 W (balanced) for shoulder internal/external, abduction/adduction, flexion/extension, and elbow flexion/extension, respectively. The comparison results imply that the power consumption in balanced condition is lower than that in unbalanced condition except the shoulder internal/external motion. In addition, the increases of body weight and height may cause higher power expenditure. According to equation (23), the residual torque acting on the shoulder internal/external joint is null, therefore, the power consumption of this joint did not change much in different conditions. As a whole, the overall power consumption of the experiments, including the tests with subject 1 and subject 2, under balanced condition decreases about 34.56% when compared to the overall power consumption under unbalanced condition. During the operation treatment, large amounts of the energy are consumed in resisting the gravity forces and inertial forces acting on the human arm and exoskeleton, and the frictional resistance of the Bowden-cable transmission system. The friction between the inner cable and outer sheath is positively correlated with the driving torque of each joint.[29,30] Therefore, the experimental results prove that the power consumption can be effectively reduced in balanced condition.

Conclusion and future works

This paper presented a gravity balanced exoskeleton with Bowden-cable actuators for the upper-limb rehabilitation of stroke patients. The mechanical

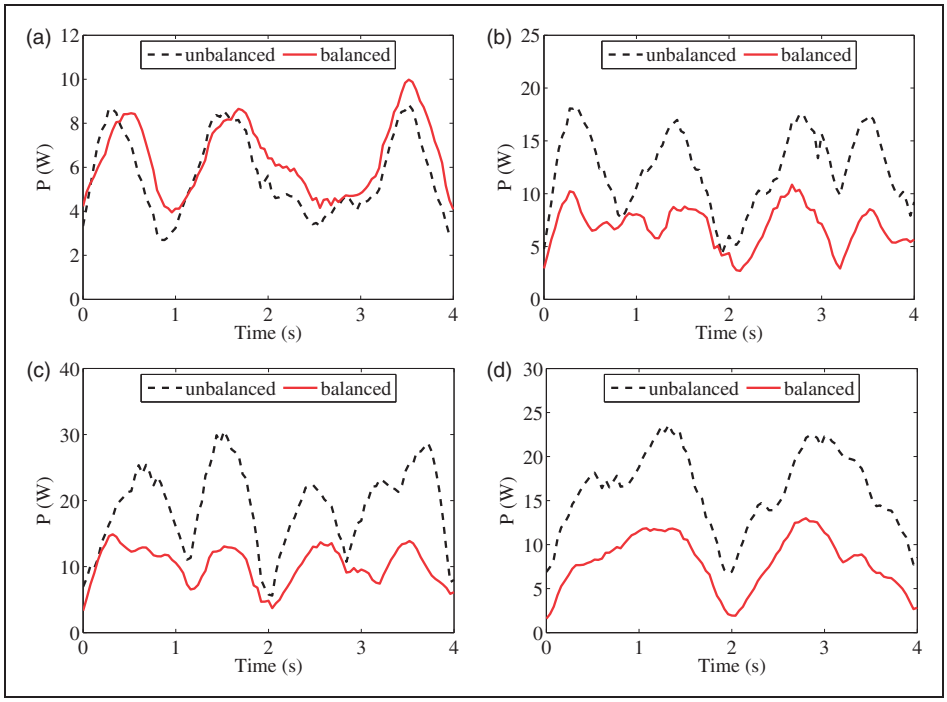

Figure 10. Power consumption of each active joint during a cycle of tracking motion (results of tests with subject 1). (a) Shoulder internal/external, (b) shoulder abduction/adduction, (c) shoulder flexion/extension, (d) elbow flexion/extension.

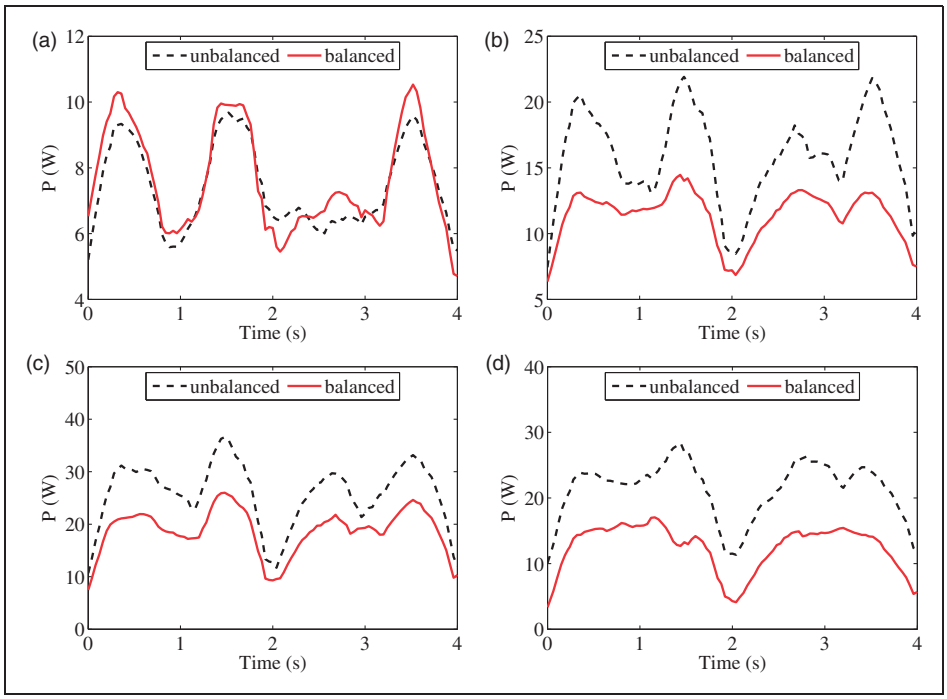

Figure 11. Power consumption of each active joint during a cycle of tracking motion (results of tests with subject 2). (a) Shoulder internal/external, (b) shoulder abduction/adduction, (c) shoulder flexion/extension, (d) elbow flexion/extension.

structure and kinematics were described and optimized to achieve good therapy performance and full workspace in ADL. The gravity balance principle was developed by utilizing auxiliary links and zero-free-length springs to locate the COM of upper limb and balance the effect of gravity with all configurations. The exoskeleton was proved to be robust to the balance errors resulting from the variation of anthropometric parameters. A real-time control system was established for the control of the exoskeleton based on Matlab/RTW. In order to validate the performance improvement made by the balanced mechanism,

two subjects with different anthropometric parameters were required to conduct the circular trajectories tracking experiments under balanced and unbalanced condition respectively. The experimental results suggest that the tracking errors can be effectively reduced with gravity balancing. Furthermore, with the balance strategy, the overall power consumption during experiments can be reduced by 34.56%. Future works will be devoted to improve mechanical structure to achieve active control of elbow pronation/supination, wrist flexion/extension, and radial/ulnar deviation. In addition, for the purpose of decreasing the balance errors resulting from the variation of anthropometric parameters, we are planning to apply the energy-free adjustment method to the design of the improved gravity equilibrators, which can help to adjust the stiffnesses and locations of the balancer springs in accordance with different individuals without need for external work.[16] Besides, control schemes for interactive rehabilitation training need to be developed to improve the therapy effectiveness.[31–34]

Declaration of Conflicting Interests

The author(s) declared no potential conflicts of interest with respect to the research, authorship, and/or publication of this article.

Funding

The author(s) disclosed receipt of the following financial support for the research, authorship, and/or publication of this article: This research has been supported by the Fundamental Research Funds for the Central Universities (CXZZ13_0085), the Scientific Research Foundation of Graduate School of Southeast University (YBJJ1427), and the China Nation Nature Science Foundation under grants 51175078 and 5087504.

References

1. Johnston SC, Mendis S and Mathers CD. Global variation in stroke burden and mortality: estimates from monitoring, surveillance, and modelling. *Lancet Neurol* 2009; 8: 345–354.
2. Dobkin BH. Strategies for stroke rehabilitation. *Lancet Neurol* 2004; 3: 528–536.
3. Reinkensmeyer DJ, Emken JL and Cramer SC. Robotics, motor learning and neurologic recovery. *Annu Rev Biomed Eng* 2004; 6: 497–525.
4. Cirstea MC and Levin MF. Compensatory strategies for reaching in stroke. *Brain* 2000; 123: 940–953.
5. Ball SJ, Brown IE and Scott SH. MEDARM: a rehabilitation robot with 5 DOF at the shoulder complex. In: *Proceedings of the 2007 IEEE/ASME international conference on advanced intelligent mechatronics*, Zurich, 2007, pp.1–6. Switzerland: *IEEE/ASME*.
6. Kwakkel G, Kollen BJ and Krebs HI. Effects of robot-assisted therapy on upper limb recovery after stroke: a systematic review. *Neurorehabil Neural Repair* 2008; 22: 111–121.
7. Krebs HI, Ferraro M, Buerger SP, et al. Rehabilitation robotics: pilot trial of a spatial extension for MIT-Manus. *J Neuroeng Rehabil* 2004; 1: 1–15.
8. Klein J, Spencer S, Allington J, et al. Optimization of a parallel shoulder mechanism to achieve a high-force, low-mass, robotic-arm exoskeleton. *IEEE Trans Robot* 2010; 26: 710–715.
9. Nef T, Mihelj M and Riener R. ARMin: a robot for patient-cooperative arm therapy. *Med Biol Eng Comput* 2007; 45: 887–900.
10. Frisoli A, Salsedo F, Bergamasco M, et al. A force-feedback exoskeleton for upper-limb rehabilitation in virtual reality. *Appl Bionics Biomech* 2009; 6: 115–126.
11. Ozkul F and Barkana DE. Upper-extremity rehabilitation robot rehabroby: methodology, design, usability and validation. *Int J Adv Robot Syst* 2013; 10: 1–13.
12. Ren Y, Park HS and Zhang LQ. Developing a whole-arm exoskeleton robot with hand opening and closing mechanism for upper limb stroke rehabilitation. In: *Proceedings of the 2009 IEEE international conference on rehabilitation robotics*, Kyoto, 2009, pp.761–765. Japan: *IEEE*.
13. Carignan C, Tang J and Roderick S. Development of an exoskeleton haptic interface for virtual task training. In: *Proceedings of the 2009 IEEE/RSJ international conference on intelligent robots and systems*, St. Louis, 2009, pp.3697–3702. USA: *IEEE*.
14. Coote S, Murphy B, Harwin W, et al. The effect of the GENTLE/s robot-mediated therapy system on arm function after stroke. *Clin Rehabil* 2008; 22: 395–405.
15. Agrawal SK and Fattah A. Gravity-balancing of spatial robotic manipulators. *Mech Mach Theory* 2004; 39: 1331–1344.
16. Barents R, Schenk M, Dorsser WD, et al. Spring-to-spring balancing as energy-free adjustment method in gravity equilibrators. *J Mech Design* 2011; 133: 061010.
17. Lin PY. Design of statically balanced spatial mechanisms with spring suspensions. *J Mech Robot* 2012; 4: 021015.
18. Lin PY, Shieh WB and Chen DZ. A stiffness matrix approach for the design of statically balanced planar articulated manipulators. *Mech Mach Theory* 2010; 45: 1877–1891.
19. Lin PY, Shieh WB and Chen DZ. Design of a gravity-balanced general spatial serial-type manipulator. *J Mech Robot* 2010; 2: 031003.
20. Sanchez RJ, Liu J, Rao S, et al. Automating arm movement training following severe stroke: functional exercises with quantitative feedback in a gravity-reduced environment. *IEEE Trans Neural Syst Rehabil Eng* 2006; 14: 378–389.
21. Stienen HA, Hekman EG, Prange GB, et al. Dampace: design of an exoskeleton for force-coordination training in upper-extremity rehabilitation. *J Med Devices* 2009; 3: 031003.
22. Herder JL, Vrijlandt N, Antonides T, et al. Principle and design of a mobile arm support for people with muscular weakness. *J Rehabil Res Dev* 2006; 43: 591.
23. Streit DA and Gilmore BJ. Perfect spring equilibrators for rotatable bodies. *J Mech Design* 1989; 111: 451–458.
24. Schiele A and Frans CT. Kinematic design to improve ergonomics in human machine interaction. *IEEE Trans Neural Syst Rehabil Eng* 2006; 14: 456–469.
25. Nef T and Riener R. Shoulder actuation mechanisms for arm rehabilitation exoskeletons. In: *Proceedings of the 2008 IEEE RAS & EMBS international conference*

on biomedical robotics and biomechatronics, Scottsdale, 2008, pp.862–868. USA: *IEEE*.
26. Siciliano B. Kinematic control of redundant robot manipulators: a tutorial. *J Intell Robot Syst* 1990; 3: 201–212.
27. Winter D. *Biomechanics and motor control of human movement*. 4th ed. Waterloo, Ontario: John Wiley & Sons, 2004, p.86.
28. Loh BG and Rosen J. Kinematic analysis of 7 degrees of freedom upper-limb exoskeleton robot with tilted shoulder abduction. *Int J Precis Eng Manuf* 2013; 14: 69–76.
29. Chen L, Wang XS and Xu WL. Inverse transmission model and compensation control of a single–tendon–sheath actuator. *IEEE Trans Ind Electron* 2014; 61: 1424–1433.
30. Wu QC, Wang XS, Chen L, et al. Transmission model and compensation control of double-tendon-sheath actuation system. *IEEE Trans Ind Electron* 2015; 62: 1599–1609.
31. Changhyun C and Sungchul K. Design of a static balancing mechanism for a serial manipulator with an unconstrained joint space using one-DOF gravity compensators. *IEEE Trans Robot* 2014; 30: 421–431.
32. Wu QC and Wang XS. Design of a gravity balanced upper limb exoskeleton with Bowden cable actuators. In: *Proceedings of the 2013 IFAC symposium on mechatronic systems*, Hangzhou, 2013, pp.679–683. China: IFAC.
33. Cho C and Kim S. Static balancer for the neck of a face robot. *Proc IMechE, Part C: J Mechanical Engineering Science* 2014; 228: 561–568.
34. Hussain S, Xie SQ and Jamwal PK. Adaptive impedance control of a robotic orthosis for gait rehabilitation. *IEEE Trans Cybern* 2013; 43: 1025–1034.